Understanding the Regulation of Chromatin by Phase Separation

A Thesis

submitted to

Indian Institute of Science Education and Research Pune

in partial fulfilment of the requirements for the

BS-MS Dual Degree Program

by

Apurva Saha

Under the guidance of

Prof. Dr. Alwin Köhler

Professor, Department of Molecular Biology

Max F. Perutz Laboratories, Vienna, Austria

Co-Supervisor: Dr. Laura Gallego Valle

PostDoc, Department of Molecular Biology

Max F. Perutz Laboratories, Vienna, Austria

Expert: Prof. Krishnapal Karmodia

Assistant Professor, Department of Biology

Indian Institute of Science Education and Research (IISER), Pune, India

CONTENTS

Certificate

This is to certify that this dissertation entitled **Understanding the Regulation of Chromatin by Phase Separation** towards the partial fulfilment of the BS-MS dual degree program at the Indian Institute of Science Education and Research, Pune represents work carried out by **Apurva Saha** at the India Institute of Science Education and Research (IISER) Pune under the supervision of **Prof. Dr. Alwin Köhler, Professor, Department of Medical Biochemistry, Max F. Perutz Laboratories, Vienna, Austria** during the academic year 2022-2022.

Prof. Dr. Alwin Köhler

(Research Supervisor)

Professor, Department of Molecular Biology

Max F. Perutz Laboratories, Vienna, Austria

Date: 31st October 2022

Prof. Dr. Alwin Köhler:

Apurva Saha:

Declaration

I hereby declare that the matter embodied in the report entitled **Understanding the Regulation of Chromatin by Phase Separation** are the results of the work carried out by me at the **Department of Medicinal Biochemistry, Max Perutz Labs**, under the supervision of **Prof. Dr. Alwin Köhler** and the same has not been submitted elsewhere for any other degree.

<div align="right">

Apurva Saha

(Fifth-Year BS-MS Dual Degree Program Student)

Department of Biology

Indian Institute of Science Education and Research (IISER), Pune

</div>

Date: 31st October 2022

Prof. Dr. Alwin Köhler:

Apurva Saha:

Acknowledgments

Abstract

Chromatin is a highly dynamic DNA-protein complex that contributes to various essential processes in eukaryotes, including packaging of genomes. The fundamental unit of chromatin, the nucleosome core particle, comprises of the complex formed by DNA wrapped around the histone octamer (two copies each of H2A, H2B, H3, H4). Modifications of either the histones or DNA can regulate structure and function of chromatin, along with other downstream processes. Among them, the monoubiquitination of H2B modulate crucial pathways in various organisms. In yeast, Lge1 is a critical protein for monoubiquitination of the 123rd lysine of H2B and undergoes liquid-liquid phase separation. This physical property of Lge1 can concentrate the substrate chromatin and the ubiquitination machinery comprising of Rad6 (E2 conjugating enzyme) and Bre1 (E3 ligase) to give rise to condensed reaction chambers *in vitro* and is critical for maintaining optimal levels of ubiquitinated H2B *in vivo*. To elucidate the molecular mechanism of this process, single-molecule studies of reconstituted nucleosomal arrays, which have been used extensively to study chromatin and its interaction with different factors, can be done. We have optimized the reconstitution of nucleosome arrays using biotinylated λ phage DNA to generate a template to analyze how Lge1-Bre1 condensates encounter DNA that is in the form of chromatin.

List of abbreviations

Amp	ampicillin
Å	angstrom
bp	base pairs
Bre1	brefeldin A sensitive protein 1
C-terminal	carboxy-terminal
Chl	chloramphenicol
DNA	deoxyribonucleic acid
DNase	deoxyribonuclease
DTT	dithiothreitol
E1	ubiquitin-activating enzyme
E2	ubiquitin-conjugating enzyme
E3	ubiquitin ligase
EDTA	ethylenediamine tetraacetic acid
Flag	Flag-tag, DYKDDDDK
g	grams
H2A	histone H2A
H2B	histone H2B
H2BK123ub1	histone H2B monoubiquitinated at lysine residue 123
H3	histone H3
H4	histone H4
His	histidine

HisTrap	HisTrap™ HP
HO	histone octamers
hr	hour
IDR	intrinsically disordered region
Da	Dalton
λ DNA	lambda phage DNA
L	litre/s
LB	lysogeny Broth
LBD	Large 1 binding domain
Lge1	Large 1
LLPS	liquid-liquid phase separation
K	lysine
m	meters
M	molar
$MgCl_2$	magnesium chloride
Milli-Q	Millipore Milli-Q lab water system
min	minute/s
NaCl	sodium chloride
N-terminal	amino-terminal
NCP	nucleosome core particle
OD	optical density
PAGE	polyacrylamide gel electrophoresis

PCR   polymerase chain reaction

pH   potential of hydrogen

PTM   post-translational modification

Qdot   quantum dot

Qdot signal   anti-flag antibody labeled with quantum dot

Rad6   radiation sensitive protein 6

RING   really interesting new gene

RNA   ribonucleic acid

RNF   RING finger

rpm   revolutions per minute

SDS   sodium dodecyl sulfate

SEC   size exclusion chromatography

TCA   trichloroacetic acid

TCEP   tris(2-carboxyethyl)phosphine

TEV   Tobacco Etch Virus protease cleavage site

TIRFM   total internal reflection fluorescence microscopy

Tris   tris(hydroxymethyl)aminomethane

Ub   ubiquitin

WAC   WW-containing domain adaptor coiled-coil

List of figures

List of tables

Table 1: Bacterial strains

Table 2: Growth Media and Composition

Table 3: Primers

Table 4: Plasmids

1. Introduction

1.1 Chromatin structure and function

Chromatin is a highly dynamic DNA-protein complex that packages the genomes tightly in eukaryotes (Figure 1). It contributes to numerous essential cellular mechanisms such as DNA replication, transcription, DNA packaging, DNA damage repair, regulation of gene expression, genetic recombination, and cell division (Quina, Buschbeck and di Croce, 2006).
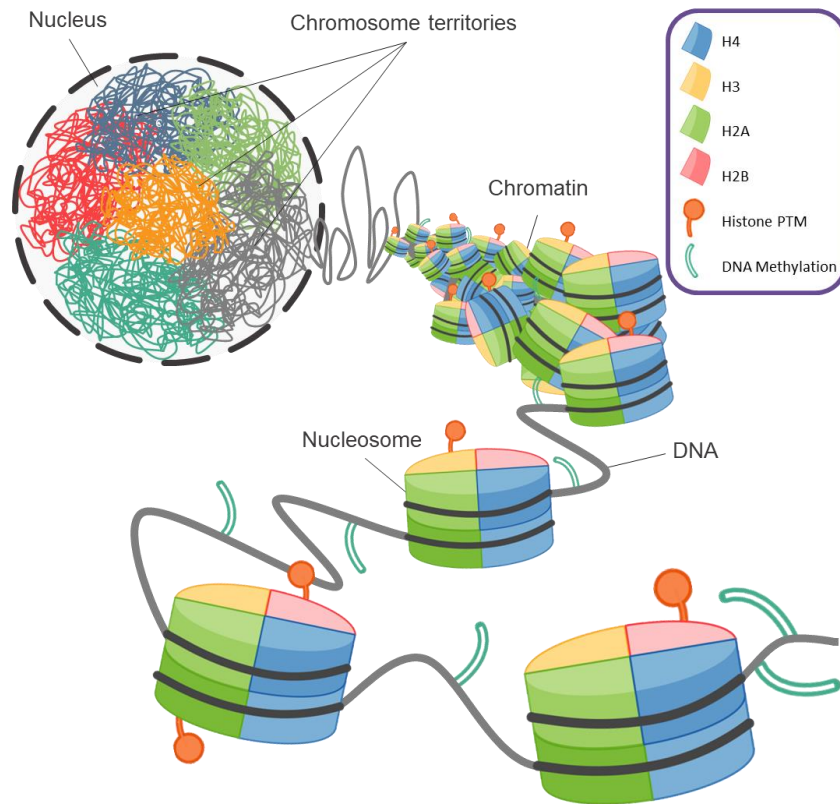
Figure 1: Schematic representation of chromatin organization in cells. The octameric nucleosome core consists of two copies of each histone: green, H2A; red, H2B; yellow, H3; blue, H4; orange, PTMs; teal, DNA methylation. Figure adapted from (Rosa and Shaw, 2013)

The fundamental unit of chromatin is the nucleosome core particle (NCP), comprising the DNA wrapped around histone proteins (Baldi, Korber and Becker, 2020) (Figure 1). The

nucleosome core particles are separated by linker DNA, forming the chromatin fibers, giving rise to the 10nm "beads-on-a-string" structure, as visualized using electron microscopy, wherein the string is the linker DNA, and the beads are the nucleosomes (Kornberg, 1974). This form of chromatin is called euchromatin, which is not packed tightly, and allows transcription factors to bind and enable gene expression (Quina, Buschbeck and di Croce, 2006).

The chromatin fiber can condense further to form higher organizational structures. This electron-dense, highly coiled, tightly packed form of chromatin is called heterochromatin. Heterochromatin can lead to gene silencing, and can influence genetic stability, cell-type specific transcription, cell differentiation, and centromere function (Quina, Buschbeck and di Croce, 2006).

1.1.1 Nucleosome core particle organization

1.1.1.1 The histone octamer organization and histone fold

The nucleosome core particle includes the DNA, which wraps around the histone octamer (two copies each of the core histones: H2A, H2B, H3, H4) (Figure 1, 2) (Mariño-Ramírez *et al.*, 2007). H3 and H4 form a tetramer and bind with the H2A-H2B dimer through two H2B-H4 interactions to form an octamer. The final octamer consists of an (H3-H4)$_2$ hetero-tetramer at the central core, with two associated hetero-dimers of (H2A-H2B) flanking it (Mariño-Ramírez *et al.*, 2007; McGinty and Tan, 2015) (Figure 2).

The interactions between histones stabilize the "histone fold," a conserved structural motif included in each histone (Mariño-Ramírez *et al.*, 2007). The fold domain is a globular structure comprised of three α helices connected by two loops. This structure allows for a "handshake motif" interaction, characteristic of the histone octamer (Mariño-Ramírez *et al.*, 2007; McGinty and Tan, 2015).

Apart from the histone fold domain, the NCP comprises of the protruding flexible N-terminal and C-terminal tails (Figure 2). These tails are variable in length and are accessible to an extensive amount of post-translational modifications (PTMs). The tails

play essential roles in nucleosome stability, chromatin compaction and dynamics, transcriptional regulation, and DNA repair (Ghoneim, Fuchs and Musselman, 2021).

The N-terminal tails from H2B and H3 protrude from the nucleosome core and pass between the two DNA strands and thus are freely subjected to different modifications (McGinty and Tan, 2015) (Figure 2). The N-terminal tail of H4 (Figure 2), containing a patch of basic residues, can extend outside the core and interact with the acidic surface of the H2A-H2B dimers on the neighboring nucleosomes, thus being able to regulate higher-order chromatin structures (Mariño-Ramírez *et al.*, 2007) (Figure 2).

The C-terminal tail of H2A (Figure 2) stabilizes DNA wrapping and histone exchange kinetics and plays a role in nucleosome mobility. It modulates efficient nucleosome translocation by chromatin remodelers, thus making it essential for the stabilization of the core and as a mediator for interactions governing the dynamics and conformation of chromatin (Ghoneim, Fuchs and Musselman, 2021). The C-terminal of H2B plays roles in chromatin compaction (Wang *et al.*, 2011). The C-terminal tail of H4 (Figure 2) affects the core stability and nucleosome sliding *in vitro* (Nurse *et al.*, 2013) and the maintenance of stable histone octamer *in vivo* (Chavez *et al.*, 2012).
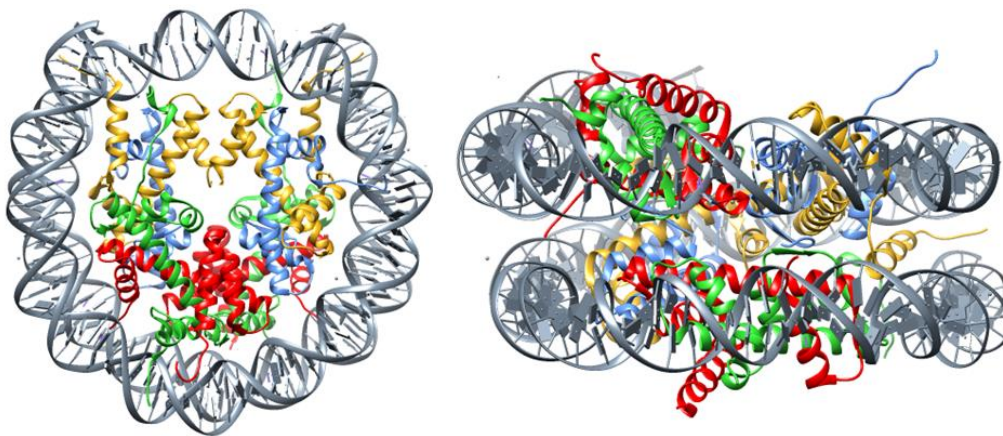
Figure 2: Structure of the NCP at 2.8 Å resolution: PDB 1ID3 (Luger et al., 2001). The ribbons represent the four histones. Grey, DNA. The top view (left) shows the disk form of the NCP bound to DNA, while the side view (right) shows the histone tails protruding out.

The tails thus play a role in the interaction of DNA with the NCP (Ghoneim, Fuchs and Musselman, 2021). Even though every DNA sequence can potentially bind to histones, there is a several-fold increase in the binding affinity for sequences enriched with periodically occurring AA, TT, or AT dinucleotides with ten base pair periodicities in counter phase with GC nucleotides (Finkelstein, Visnapuu and Greene, 2010). *In vitro* nucleosome reconstitution of chromatin takes advantage of this physical property (Ura and Kaneda, 2001).

1.1.1.2 *In vitro* assembly of the NCP

In order to study the structure and function of chromatin and its interaction with different factors, DNA templates have been used extensively to reconstitute nucleosomal arrays. Such an array serves appropriate for studying chromatin-like structures, and DNA-protein interactions on substrates that have nucleosomes. This is because DNA-directed processes involve chromatin rather than naked DNA *in vivo*. NCP arrays can be used to investigate how molecules of interest interact with chromatin, or influence nucleosome stability and positioning, chromatin structure, and function (Lusser and Kadonaga, 2004).

Extensively studied nucleosome positioning sequences from eukaryotic species are used for *in vivo* studies, such as the satellite DNAs. They consist of tandem repeats of sequences up to 500 bp, and are used to give rise to NCP arrays with regularly spaced nucleosomes (Ura and Kaneda, 2001; Bussiek *et al.*, 2007). They have been used to understand histone-DNA and protein-chromatin interactions, higher-order chromatin structures and transcription, and role of DNA sequences in histone octamer positioning and, ultimately, gene regulation (Ura and Kaneda, 2001; Bussiek *et al.*, 2007; Gallego *et al.*, 2020).

In vitro, one of the most prevalently used methods to assemble histones on DNA or plasmids is the salt dialysis method (Lusser and Kadonaga, 2004; Gibson *et al.*, 2019; Gallego *et al.*, 2020). It entails the mixing purified core histones and DNA, followed by

dialysis in a buffer starting from a high to a low ionic strength of salt (Ura and Kaneda, 2001). This form of nucleosome assembly is random because the spacing between the nucleosomes could be of variable length, unlike the physiological length of approximately 200 bp, if DNA sequences with no nucleosome positioning sequences are used (Lusser and Kadonaga, 2004). However, reconstitution of chromatin with regularly spaced nucleosomes could be made possible by using specific DNA templates with well-defined tandem repetitive sequences, which have a strong affinity for nucleosomes (Lowary and Widom, 1998).

The artificial 601 sequence has a strong affinity towards a single histone octamer and is used extensively for studying nucleosome structure, PTM modifications, and function *in vitro* (Gibson *et al.*, 2019; Gallego *et al.*, 2020). In the 601 sequence, there are 282 bp, 147 bp of which have a high affinity towards the histone octamer. The rest 135 bp flanking regions on either side of this core sequence make up the nucleosome-free region (Lowary and Widom, 1998). Tandem repeats of these 601 sequences can reconstitute nucleosomal arrays that consist of a specific number of nucleosomes at a regular interval. One can control the number of nucleosomes on the fiber by changing the number of repeats (Lowary and Widom, 1998; Ura and Kaneda, 2001).

While tight chromatin fibers are helpful for some applications, increasing the length of the DNA template is required for higher-resolution techniques, such as in single-molecule studies. Single-molecule studies include techniques that visualize an ensemble of individually tagged fluorescent proteins in real-time (Fazio *et al.*, 2008). With this resolution, many biophysical parameters of single proteins or complexes regulating chromatin can be studied, for example, the transcription speed of polymerases (Davidson *et al.*, 2016), road-blocks that prevent protein sliding on DNA (Finkelstein, Visnapuu and Greene, 2010; Davidson *et al.*, 2016), and the forces applied by chromatin regulators (Fazio *et al.*, 2008). There are two main techniques for single molecule resolution: optical tweezers and DNA curtain assays (Collins *et al.*, 2014; Morin *et al.*, 2020). In the method using optical tweezers, DNA is stretched between beads, and interactions with different molecules are tested. DNA curtain assays, on the other hand, comprise of aligning thousands of DNA molecules in a flow chamber on a slide to visualize and analyze

protein-nucleic acid interaction at the level of a single molecule in real-time (Collins *et al.*, 2014).

To reach such a resolution, the WIDOM 601 sequence has also been inserted in pPlat to do single molecule studies (Gibson *et al.*, 2019) and to study how single nucleosomes inserted in specific positions act as road-blocks for different chromatin regulator proteins (Davidson et al., 2016). Still, the disadvantage of such a system is that the fiber length is suboptimal when specific processes are studied (Gibson *et al.*, 2019). Another DNA substrate used widely for chromatin reconstitution for single-molecule studies is the lambda phage DNA (λ-DNA , ~48.5 kbp). λ-DNA has a wide sequence variety rising from the naturally occurring A-T rich and G-C rich halves due to the exclusionary poly (dA-dT) tracts around the center of the fiber, which play a dominant role in nucleosome positioning (Visnapuu and Greene, 2009). It does not have an evolutionary pressure to position nucleosomes. Still, when stretched, it can reach 10-12μm (Visnapuu and Greene, 2009), which is an appropriate size for studying single-molecule biophysics.

1.1.2 The PTMs of chromatin

Histones are modified post-translationally for various regulatory processes. The flexible tails undergo various reversible PTMs, including methylation, acetylation, ubiquitination, SUMOylation, and phosphorylation (Bannister and Kouzarides, 2011). These modifications are part of the epigenome and play an essential role in replication, transcription, gene expression, gene activity, silencing, chromatin assembly, and DNA modifications and repair (Bannister and Kouzarides, 2011).

1.1.3 Chromatin ubiquitination

1.1.3.1 The molecular mechanism of ubiquitination

Ubiquitination is a process in which the 76 amino acid polypeptide ubiquitin attaches to substrates for various functions. It is involved in targeting proteins for proteasomal

degradation and cell signaling and plays roles in regulating transcription, maintaining chromatin structure, DNA damage response, and endosomal sorting (Cao and Yan, 2012).

The targeting of proteins for ubiquitination begins in an ATP-dependent manner wherein the ubiquitin-activating enzyme (E1) "activates" ubiquitin and transfers ubiquitin to the cysteine residue of E1. The activated ubiquitin is then transferred to the active site cysteine of a ubiquitin-conjugating enzyme (E2), generating an E2~Ub conjugate from the transferred activated ubiquitin. Finally, the ubiquitination of the protein substrates involves the activity of the ubiquitin-protein ligase (E3). The transfer could either be direct, which means the ubiquitin is directly transferred from the E2~Ub conjugate to the protein by the action of the E3, or via a thioester linkage between Ub and E3. In any case, ubiquitination relies on the covalent linkage of ubiquitin to the lysine, serine, threonine, or cysteine residues of the protein substrate or the N-terminus of the protein (Callis, 2014).

Target proteins can undergo either monoubiquitination or polyubiquitination. Monoubiquitination is the conjugation of a single ubiquitin moiety to the substrate and is primarily associated with chromatin regulation, protein sorting, and trafficking. Polyubiquitination is the process that consists of multiple monoubiquitination events occurring on the same or different residues of the substrate and is mainly linked with proteasomal or autophagic degradation for protein signaling (Cao and Yan, 2012; Callis, 2014).

The modifications of the histones regulate critical cellular processes such as the expression of genes and the repair of DNA. Anomalies regulating optimal ubiquitin levels can often lead to diseases like cancer. Several enzymes that modify histones are oncogenes or tumor suppressors (Ciechanover and Schwartz, 1998; Cao and Yan, 2012; Callis, 2014).

1.1.3.2 H2BK123 monoubiquitination in *Saccharomyces cerevisiae*

In yeast, H2B is monoubiquitinated at lysine 123 (H2BK123ub1) (Cucinotta *et al.*, 2015) (which corresponds to K120 in humans). Histone monoubiquitination is a process that is conserved from yeast to mammals. This modification plays critical roles in DNA replication, transcriptional regulation, modifications of other histones, nucleosomal organization, DNA repair, apoptosis, and cell size control. (Zhu, Zheng, A. D. Pham, *et al.*, 2005; Nakanishi *et al.*, 2009).

The three proteins involved in the ubiquitination machinery of H2BK123ub1 in *Saccharomyces cerevisiae* are the E2 conjugating enzyme Rad6 (radiation sensitive protein 6) (Koken *et al.*, 1991) and the E3 ligase Bre1 (brefeldin A sensitive protein 1) (Hwang *et al.*, 2003; Wood *et al.*, 2003), which interacts with the protein Lge1 (Large 1) (Song and Ahn, 2010; Gallego *et al.*, 2020). Although all three proteins are conserved in *Schizosaccharomyces pombe* (Reynolds *et al.*, 1990; Elmore *et al.*, 2014), in humans, only the orthologs for Rad6 (RAD6A, RAD6B) and Bre1 (RNF20/RNF40) have been found (Zhu et al., 2005), which ubiquitinates the analogous H2BK120 (Deng *et al.*, 2020). However, RNF20/RNF40 interacts with WW-containing domain adaptor coiled-coil (WAC) (WW- containing domain adaptor coiled-coil works as a functional partner for RNF20/RNF40) (Zhang and Yu, 2011), which is a protein that shares structural and functional similarities with Lge1 (Gallego *et al.*, 2020).

Bre1 is a RING (really interesting new gene) E3 ligase that has a RING domain at its C-terminal (Figure 3B) that promotes the association of Bre1 to the Rad6~Ub conjugated complex and the NCP (Turco *et al.*, 2015). Bre1 also establishes a second interaction with Rad6 via an N-terminal Rad6 binding domain which facilitates ubiquitin transfer (Deng *et al.*, 2020) (Figure 3B). Bre1 also interacts with Lge1 through the Lge1-binding Domain (LBD) (Song and Ahn, 2010; Gallego *et al.*, 2020) (Figure 3B). Lge1 is an essential protein for H2BK123ub1 that undergoes liquid-liquid phase separation mediated by multivalent interactions of its intrinsically disordered N-terminal domain (Figure 3A, 3C). Lge1-Bre1 interaction gives rise to a core-shell membrane-less compartment wherein Bre1 forms the catalytic shell around a liquid-like Lge1 core (Figure 3C). Lge1

can lead to the ubiquitination machinery's concentration by forming condensed reaction chambers *in vitro*. In vivo, Lge1 phase separation maintains optimal levels of H2BK123ub1 in gene bodies (Gallego *et al.,* 2020) (Figure 3C).

Conclusively, Lge1-Bre1 forms core-shell condensates wherein Bre1 plays a direct catalytic role, and the core concentrates E2 Rad6 and the chromatin substrate. This leads to the confinement of the reactants in a small space at a high concentration, thus increasing the opportunity for productive interaction. These histone ubiquitination hubs can target gene body nucleosomes and regulate gene architecture and expression (Gallego et al., 2020) (Figure 3C).
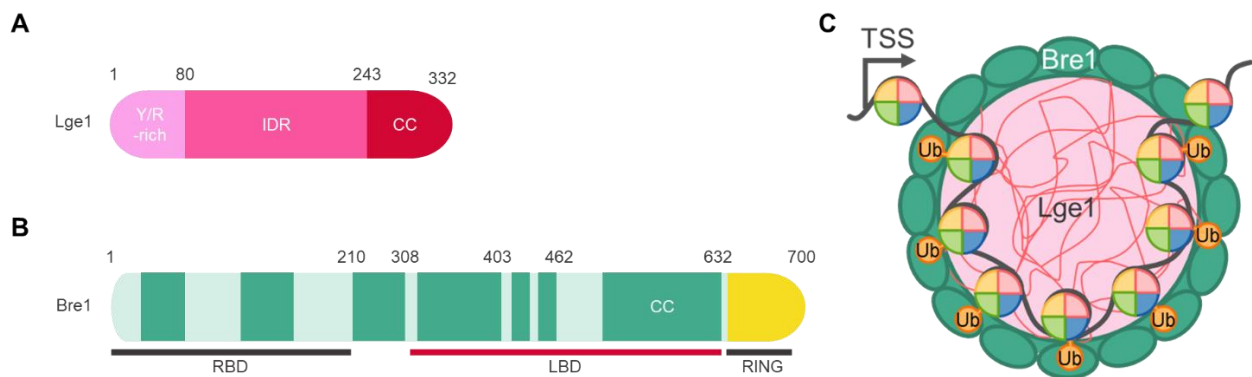
Figure 3: H2BK123ub1 by Rad6, Bre1, and Lge1. (A) Domain organization of Lge1 drawn to scale. Y/R-rich sticker region (1-80). IDR, Intrinsically Disordered Region (1-242). CC, Coiled-Coil domain (red). **(B)** Domain organization of Lge1 and Bre1 drawn to scale. CC, coiled-coil domain (green; non-coiled-coil regions, grey); LBD, Lge1-binding domain; RBD, Rad6-binding domain; RING, really interesting new gene domain. **(C)** Current LLPS-based ubiquitination model. The chromatin fiber is ubiquitinated in the core-shell structure mediated by Bre1. NCP colored as in Figure 1. The figure was adapted from (Gallego *et al.*, 2020).

1.2 Biomolecular condensates: types of condensates, liquid-liquid phase separation (LLPS), and its roles

Eukaryotic cells comprise various membrane-bound and membrane-less compartments. Membrane-bound compartments include the Golgi apparatus, endoplasmic reticulum, mitochondria, nucleus, lysosomes, endosomes, and peroxisomes. Membrane-less compartments include the centrosome, Cajal bodies, nucleolus, different granules, and many more (Banani et al., 2017) (Figure 4A).

LLPS entails a process in which the solute molecule that distributes homogenously separates into two compartments of different solute concentrations to reach chemical equilibrium leading to highly condensed structures. This gives rise to a phase-separated system consisting of a solute-rich compartment within a large diluted solvent phase (Hyman, Weber and Jülicher, 2014; Banani et al., 2017). Phase separation can be induced by changes in temperature, concentration, post-translational modifications, etc. (Banani et al. 2017) (Figure 4B).
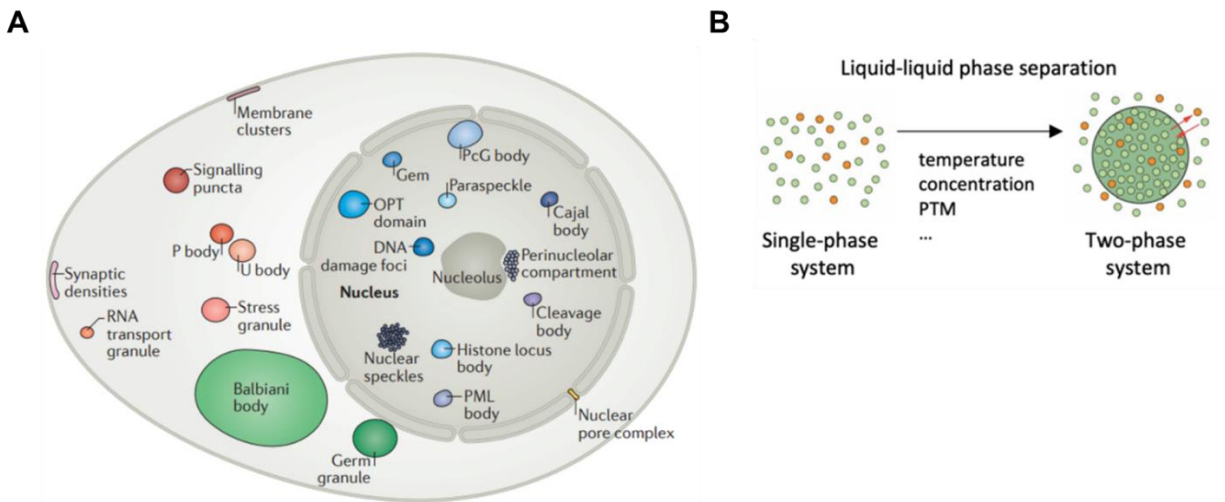
Figure 4: LLPS and biomolecular condensates in eukaryotic cells. (A) Scheme of liquid-liquid phase separation (LLPS). Molecules in a single-phase solution assemble in a highly condensed droplet, forming a separate new phase. Molecules exchange between the condensate and the surrounding dilute phase. The figure is from (Banani et al., 2017) **(B)** Variety of biomolecular condensates in eukaryotic cells. Condensates can be in the nucleus, cytoplasm, and on membranes. Balbiani bodies and germ granules are

only found in germ cells. RNA transport granules and synaptic densities are exclusive to neuronal cells—figure from (Banani et al., 2017).

Proteins with IDRs, with low sequence complexity and rich in aromatic acids and charged residues, can phase separate, regardless of the involvement of nucleic acids, in physiological conditions (Banani et al., 2017).

IDRs do not have a specific three-dimensional conformation but consist of repetitive sequences that contribute to multivalent interactions that seed phase separation. Biomolecular interactions, such as electrostatic interaction, hydrophobic π-stacking, and hydrogen bonds, are factors that can regulate such a phenomenon. In addition to IDRs, multivalent interactions stemming from folded protein domains, nucleic acids, and chromatin are the driving factors for phase separation. The interactions due to such factors could be regulated by PTMs, binding interactions, and environmental conditions (Hyman, Weber and Jülicher, 2014; Banani et al., 2017).

In cellular environments, biomolecular condensates play a role in various structural and functional processes. They regulate enzyme kinetics by concentrating or segregating the reaction components, modulating the specificity of biochemical reactions, supporting the assembly of macromolecular complexes, and playing a role in signaling, protein homeostasis, or sub-compartmentalization (Banani et al., 2017). Phase separation has also been suggested to regulate chromatin-related processes (Hyman, Weber and Jülicher, 2014; Banani et al., 2017; Lyon, Peeples and Rosen, 2021).

1.2.1 LLPS in chromatin-related process

Chromatin resembles many macromolecules that are known to undergo LLPS. Chromatin and the components involved in PTMs undergo LLPS to govern chromatin organization and function (Sanulli *et al.*, 2019). However, it is unclear whether histones can phase separate or whether the higher-order structures are in the form of a 30 nm fiber or a more

disordered state. The core histones and the linker histone H1, which can directly contribute to LLPS of heterochromatin in cells, consist of IDRs that make up about 50% of the protein and possess a significant net positive charge (Shakya et al., 2020). Interestingly, only H2A can undergo LLPS with DNA, forming liquid-like droplets, unlike the other three core histones, which precipitate *in vitro* (Shakya et al., 2020). The H2A C-terminal tail is thought to be contributing to this behavior as it has a higher percentage of residues that are capable of hydrogen bonding, suggesting that just the overall charge and disordered-ness are not contingent for determining LLPS (Gibson et al., 2019; Shakya et al., 2020).

Condensation could also possibly regulate chromatin structure. For example, there has been a proposition that condensates can play a role in bringing distant target chromatin regions to reorganize chromatin, facilitating several biological processes (Sanulli *et al.*, 2019). LLPS can also facilitate the maintenance of euchromatin and heterochromatin regions of chromatin through proteins like HP1α. This protein modulates heterochromatin formation through phase separation and can dynamically compact chromatin to drive the LLPS of chromatin (Gibson *et al.*, 2019; Sanulli *et al.*, 2019).

Phase separation is also debated to be involved in regulating transcription-related processes. Nuclear speckles sequester transcription factors inhibiting transcription (Galganski, Urbanek and Krzyzosiak, 2017). Other transcription factors and super-enhancers have also been proposed to undergo LLPS to form active foci for their transcriptional activity (Ann Boija *et al.*, 2018; Wagh, Garcia and Upadhyaya, 2021). RNA Polymerase II can undergo phase separation via its intrinsically disordered C-terminal domain (CTD), which can govern its initiation and elongation (Boehning *et al.*, 2018). There is still a debacle about whether the entire transcriptional machinery could organize itself via phase separation or alternative regulation pathways.

2. Goals for this project and previous experiments

Lge1-Bre1 condensates are thought to interact with the chromatin fiber during H2B ubiquitination and therefore are likely to be in direct contact with DNA and histones. Dr. Laura D. Gallego, who works in the group of Prof. Dr. Alwin Köhler at the Max-Perutz-Labs in Vienna, performed *in vitro* experiments that showed that Lge1-Bre1 condensates indeed bind to DNA and are even able to compact long DNA fibers (unpublished data). This compaction is not present in the presence of Bre1 alone, indicating that Lge1-driven LLPS might be essential for this compaction.

To replicate the *in vivo* condition where DNA is in the form of chromatin and reconstitute a template that the Lge1-Bre1 condensates are likely to encounter, we aimed to:

1. Optimize the reconstitution of nucleosome arrays using biotinylated λ phage DNA

2. Analyze how Lge1-Bre1 condensates encounter DNA that is in the form of chromatin

To investigate this, we intended to set up an approach called DNA curtain assays using nucleosome arrays. This would allow us to visualize the behavior of proteins of interest on tethered nucleosome arrays *in vitro* at a single molecule resolution.

In the second part of this project, we wanted to further elucidate the role of histone tails in the partitioning of chromatin in Lge1-Bre1 condensates. We already know that the reconstituted 16-unit NCP array also gets rapidly recruited to the shell of the Lge1-Bre1 condensates and partially diffuses into the core over time. Moreover, histone tails play an essential role in chromatin signaling, and thus, we planned to:

3. Analyze how the histone tails encounter Lge-Bre1 condensates and what kind of partitioning behavior they show upon that.

To investigate this, we intended to tag the N-terminal tails of yeast histone H2A, H2B, H3, and H4 and the C-terminal tail of H2A with mGFP and analyze their behavior when they encounter Lge1-Bre1 condensate *in vitro*.

3. Materials and methods

3.1. Materials

3.1.1 Bacterial Strains

All bacterial strains used during this study are listed in Table 1.

Table 1: Bacterial strains

Strain	Genotype
DH5 alpha	fhuA2 lac(del)U169 phoA glnV44 Φ80' lacZ(del)M15 gyrA96 recA1 relA1 endA1 thi-1 hsdR17
BL21-CodonPlus (DE3)-RIL	E. coli B F-ompT hsdS(rB- mB-) dcm+ Tetr gal λ (DE3) endA Hte [argU ileY leuW Camr]

3.1.2 Media and Growth Conditions

Bacteria were cultivated on LB plates or in liquid LB medium in standard conditions at 37°C (Sambrook, Fritsch and Maniatis, 1989). Liquid cultures were grown under constant shaking of 150rpm. The composition or source of growth media used during this study are listed in Table 2.

Table 2: Growth Media and Composition

Medium	Composition or Source
Luria Bertani Broth (LB), Miller (Miller Luria Bertani Broth) - HIMEDIA	Ingredients (g/L): Tryptone (10), Yeast extract (5), Sodium chloride (10), Final pH (at 25°C) 7.5±0.2 Prepared using 25g per 1L of purified/distilled water
LB plates	Supplied by institute

LB+Amp plates	Supplied by institute (100 mg/L ampicillin)
LB+Amp medium	LB medium, 100 mg/L ampicillin
LB+Amp +Chl medium	LB medium, 100 mg/L ampicillin, 34 mg/L chloramphenicol

3.1.3 Primers

All primers generated during this study are listed in Table 3.

Table 3: Primers

Standard Cloning Primers	
H4 N-terminal tail FP	ATGAAGGATCCagCGGTAGAGGTAAAGGTGGT
H4 N-terminal tail RP	GGTAAGTCGACATTCTTAGAATCTTgcgGTGACG
H3 N-terminal tail FP	ATGAAGGATCCGCcAGAACAAAaCAAACAGCA
H3 N-terminal tail RP	AATTAGTCGACGCAGGCTTCTTAACACCACCGGT
H2A N-terminal tail FP	ATGAAGGATCCTCTGGTGGTAAAGGTGGTAAA
H2A N-terminal tail RP	ATGAAGTCGACGCAGCAGAaCGAGATTGAGAcGC
H2A C-terminal tail FP	ATGAAGGATCCTCTGCCAAGGCcACCAAaGCTTCTCAAGAATTATAATAGTCGACGCAGA
H2A C-terminal tail RP	TCTGCGTCGACTATTATAATTCTTGAGAAGCtTTGGTgGCcTTGGCAGAGGATCCTTCAT
H2B N-terminal tail FP	ATGATGGATCCTCCTCTGCCGCCGAAAAGAAA
H2B N-terminal tail RP	ATGAAGTCGACGCACCATCtACGGAGGTTGAaGT
FastCloning Primers	
H4 N-terminal tail FP	CTAGGAAAAGGTGGTGCCAAGCGTCACAGAAAGATTCTAAGAATGTCGACGTCTAAAGGTGAAGAATT
H4 N-terminal tail RP	ACCACCTTTTCCTAGACCTTTACCACCTTTACCcCTACCaGAGGATCCCATGGCGCCCTGAAAATA
H2A N-terminal tail FP	GCTGGTTCAGCTGCTAAAGCcTCTCAATCTCGCTCTGCTATGTCGACGTCTAAAGGTGAAGAATT

H2A N-terminal tail RP	AGCAGCTGAACCAGCTTTACCACCTTTACCACCaGAG GATCCCATGGCGCCCTGAAAATA

3.1.4 Plasmids

Table 4 lists all plasmids that were either available in the laboratory's plasmid collection or during this study.

Table 4: Plasmids

Plasmid	Vector	Antibiotic resistance
HHF2 (H4)	pST50-Trc1-HISNDHFR	Amp
HTA1 (H2A)	pST50-Trc2-HISNDHFR	Amp
His-TEV-FLAG-HTB2 (H2B)	pST50-Trc3-HISNDHFR	Amp
HHT1 (H3)	pST50-Trc4-HISNDHFR	Amp
pST44 HHF2-HHT1-HTA1-HIS-FLAG-HTB2	pST44	Amp
pPROEX HTb with mGFP	pPROEX	Amp

3.2 Methods

3.2.1 Transformation of *E.coli*

Both strains used in the study, BL21 Codon+ for protein expression and DH5alpha for cloning, were transformed as follows. Chemically competent cells were mixed with 200ng DNA and incubated for 30 min on ice. After a heat shock of 45 s at 42°C, the cells were recovered for 30 min in 200 µl LB, transferred into LB+Amp +Chl, and grown overnight.

3.2.2 Cloning

mGFP-tagged H3 N-terminal tail and H2B N-terminal tail clones with pPROEX HTb vector containing mGFP and StrepII were constructed using PCR cloning.

3.2.2.1 FastCloning approach

The FastCloning technique was used for attempting to clone the H4 N-terminal tail and H2A N-terminal tail as described in (Li et al., 2011).

3.2.3 Nucleosome array reconstitution for 601WIDOM sequence

Reconstitution of nucleosomal arrays using 601WIDOM was done as described in (Gallego *et al.*, 2020).

3.2.4 Reconstitution of nucleosome arrays for biotinylated λ DNA

3.2.4.1 Biotinylation of λ DNA

λ phage DNA (NEB, #N3011S) was biotinylated in the single end or both ends following the protocol described in (Yardimci *et al.*, 2012).

3.2.4.2 Recombinant protein expression

E. coli BL21 Codon Plus (DE3) RIL cells were used for expressing proteins. Expression vectors were transformed and grown at 37°C until an OD of 0.6. It was then transferred to a shaker at 23°C and grown until an OD of 0.8. Induction for expression was done by adding 0.5x IPTG followed by shaking at 23°C for 3hrs. Cells were harvested by centrifuging at 4500rpm for 12min and resuspended in Milli-Q water. Cells were then pelleted at 4500rpm for 15min and fast-frozen in liquid nitrogen and stored at -20°C.

3.2.4.3 Recombinant protein purification

Co-expression followed by single step purification was done to generate His-TEV-Flag-Histone octamer as described in (Gallego et al., 2020). The lysis of pellets obtained after expression was done in HO buffer (50mM Tris-HCl pH 7.5, 1M NaCl, 1.5mM $MgCl_2$, 50mM Imidazole pH 7.5). Protein was purified in a HisTrap™ HP 5mL column (# 95056-206, GE Healthcare) using the ÄKTA™pure UPC 10 (#28-4062-68, GE Healthcare). The protein complex was washed using 110mL of HO buffer and eluted with buffer containing (50mM Tris-HCl pH 7.5, 1M NaCl, 1.5mM $MgCl_2$, 500mM Imidazole pH 7.5). The sample was then centrifuged at 14000rpm for 3 min at 4°C and then loaded on a SEC column (HiLoad™ 16/60 Superdex™ 200 pg) using an ÄKTA™pure (#28317, GE Healthcare)

equilibrated with buffer containing 1M NaCl, 50mM Tris pH 7.5 and 1mM EDTA followed by centrifugation for 5 min at 14000rpm at 4°C. The fractions of interest were mixed and concentrated for 7 min in Amicon Ultra-15, PLTK Ultracel-PL Membrane, 30 kDa (#UFC903024, Merck) until the final volume was 250 µL. Bradford assay was used to measure the concentration according to manufacturer's instructions and immediately used for NCP reconstitution.

3.2.4.4 Bradford assay

For Bradford assays, 990 µl Bradford solution (consisting of 20% protein assay dye (BioRad, 500-0006) in water) was mixed with 10µl of 1:1, 1:5, and 1:10 dilutions of protein, and light absorption at 595 nm was measured. To calculate protein concentrations, a reference was generated using absorption values of 10µl BSA solutions with concentrations of 0.1, 0.2, 0.3, 0.6, 1.0 and 2.0 mg/ml in 990 µl Bradford solution.

3.2.4.5 Nucleosome core particle reconstitution for biotinylated λ DNA

The entire sample with HO obtained after concentration was mixed with biotinylated λ DNA till the final reaction volume was 600µL. The sample was added to dialysis chambers Slide-A-Lyzer™ MINI Dialysis Devices, 3.5K MWCO (#88400, Thermo Fisher Scientific). The dialysis was started in buffer containing 10mM Tris-HCl pH 7.5, 2M KCl, 1mM EDTA, 1mM TCEP and exchanged with buffer containing 10mM Tris-HCl pH 7.5, 250mM KCl, 1 mM EDTA, 1mM TCEP over a time period of 18 h, using a peristaltic pump. Reconstituted NCPs were then transferred to a clean Eppendorf tube and centrifuged for 5min at 14000rpm at 4°C.

3.2.4.6 Agarose gel electrophoresis

DNA fragment sizes were analyzed by separating the fragments electrophoretically on agarose gels. Agarose gels (ranging from 0.5% to 2.5% agarose) with 4% of DNA stain RedSafe (#21141, JH Science) in TAE buffer (40mM Tris, 1.15% acetic acid, 1mM EDTA pH 8.0) were used. Running was done at 60V for 45min for DNA separation. As reference, a 50 bp (#MWD50, FastGene) or a 1 kbp DNA ladder (#SM0311, Thermo) was used.

3.2.4.7 SDS-PAGE and Coomassie staining

Extracted and purified proteins were separated according to their size using SDS-PAGE (Laemmli, 1970). 20µL of the protein sample (other than the reconstituted NCP array) was taken, and 4x sample buffer (120mM, Tris-HCl pH 6.8, 4% SDS, 20% Glycerol, and 0.01% Bromphenolblau) was added. This sample was then heated at 95°C for 5 minutes and spun down at 13000xg for 30 seconds. All proteins were separated in 12% SDS-PAGE gels. Samples containing HO or reconstituted NCP were run in NuPAGE™ MES SDS Running Buffer (20X) (Thermo Fisher Scientific #NP0002). Gels loaded with cell lysates or proteins were run in SDS running buffer (25 mM Tris, 192 mM glycine, 7.44 g/L EDTA, 1g/L SDS) at 180V for 50min and fixed in a solution containing 40% methanol and 2% acetic acid for 20 min. PageRuler (#26616, Thermo) was also loaded on each gel as a size reference. The proteins were stained with Coomassie solution (10% orthophosphoric acid, 10% w/v ammonium sulfate, 0.12% w/v Brilliant Blue, and 20% methanol (Candiano *et al.*, 2004)) for 18hrs. The gels were then washed in water and imaged with using a Chemidoc (#17001401, Bio-Rad).

3.2.4.8 TCA precipitation

The reconstituted NCP arrays were loaded onto PAGE gels after TCA precipitation. 200µL to 300µL (according to available sample volume) was taken, and TCA was added to a final 10% concentration and incubated in ice for 1 hour. The sample was then centrifuged at 14000rpm for 10 min at 4°C. The supernatant was discarded, and 400µL of 100% acetone was added, and the sample was spun at 14000rpm for 10 min at 4°C. This step was repeated twice the supernatant was discarded, and the pellet was air-dried for 20min. Finally, 25µL of 2x sample buffer (120mM, Tris-HCl pH 6.8, 200mM DTT, 4% SDS, 20% Glycerol, and 0.01% Bromphenolblau) was added and processed as mentioned in materials and methods 2.2.6.

3.2.4.9 DNA curtain assays

In this approach, DNA fibres are anchored in a microfluidic chamber which can be flushed with a buffer that contains chosen proteins. The chamber can be imaged in

real-time, and protein behavior on the tethered DNA fibers can be observed. Flow chamber assembly and surface coating: The microfluidic chamber was assembled as previously described (Yardimci *et al.*, 2012; Davidson *et al.*, 2016). In brief, biotinylated coverslips (#Bio_01_GC-MIC, Stratech) were attached to a glass slide using double-sided adhesive tape (#GBL620001-1EA, Sigma), which created a flow chamber with the dimensions of 20 x 3 x 0.12mm. Polyethylene tubes (#427416, Intramedic) (with 12cm length and 0.76mm inner diameter) were inserted into two holes in the glass slide (with 1.25mm diameter) and used as flow inlet and outlet. Leakage and air inflow was prevented by sealing the chamber with epoxy glue. Next, the chamber was incubated for 15min with 10µl avidin (1 mg/ml) (#VECA-3100, Szabo-Scandic), which binds to the biotinylated surface of the cover slip and concomitantly creates a binding surface for biotinylated DNA templates (Wilchek and Bayer, 1990).To prevent protein fouling on the glass surface, the glass was subsequently passivated by incubating the chamber with 1% Pluronic F-127 (#P2443-250G, Sigma) for ≥ 1 h (Li *et al.*, 2019)

### 3.2.4.10 Total internal reflection fluorescence microscopy

For imaging of DNA curtains, TIRFM was used. This type of microscopy relies on total light reflection that occurs when light hits a glass-water interface at a very flat angle. However, the light is not entirely reflected, but penetrates the sample for » 150 nm, creating an evanescent field that excites only fluorophores in the water phase that is close to the interface (Fish, 2009; Mattheyses, Simon and Rappoport, 2010). Curtain assays were imaged with a cellSens TIRF unit (Olympus) that was coupled to Plan-Apochromat 60x/1.42 Oil, WD 0.15 mm objective. Images were acquired with an ImagEM X2 EM-CCD camera (Hamamatsu) and processed with ImageJ. The chambers were flushed with TIRF buffer (50 mM Tris pH 8, 50 mM NaCl) for 3 min at 100µL/min. SYTOX™ Orange Nucleic Acid Stain (Thermo Fisher Scientific, #S11368) was used to visualize DNA, and Anti-Flag labeled with Qdot (Thermo Fisher Scientific, # S10454) was used for visualizing the nucleosomes. Imaging was done with filter 561 for Sytox Orange and 488/647 for Anti-Flag antibody labeled with Qdots. Time lapses were imaged for both channels every 4 seconds for 5 min. 45pM of DNA and 0.5nM of Anti-Flag labeled with Qdot was used for

the assays. Two methods were used for injection. The first one is sequential, wherein 45pM of DNA was injected at 20L/min for 5min, followed by injection of 0.5nM of Anti-Flag labeled with Qdot at 10µL/min for 7min. This was incubated for 5min, washed with TIRF buffer supplemented with Sytox Orange for 80µL at 40µL/min, and then imaged. Alternatively, 45pM of DNA and 0.5nM of Anti-Flag labeled with Qdot in a final volume of 300µL of TIRF buffer was incubated for 10min at room temperature. Injection of 80µL of the sample was done at 20µL for 5min followed by a wash with TIRF buffer at 40µL/min for 3min.

4. Results and discussion

4.1 Adaptation of protocol for chromatin reconstitution using λ DNA as template

The protocol for reconstitution of the NCP array using the 16x WIDOM sequence has been established in the lab (Supplementary Figure 1A, 1B) (Gallego *et al.*, 2020). Initially, the same experimental steps were implemented on λ DNA to reconstitute the NCP array consisting of λ DNA (Supplementary Figure 1C, 1D). The reconstitution of the 16x601 WIDOM sequence was successful as the reconstituted fiber migrated in the gel above the undigested fragment (Figure 5A, Lane 1 vs. Lane 3, Supplementary Figure 1B). As a control, ScaI digestion of the fiber was performed. If there is full occupancy of NCP in the DNA fiber, no free 601WIDOM sequence would be observed (size 247bp), but rather, a heterogeneous population of fragments greater than 200 bp due to nucleosomes can be seen (Figure 5A, Lane 4). But strikingly, when the reconstitution was done using biotinylated λ phage DNA, the product was completely degraded (Figure 5B, Lane 1 vs. Lane 2, Supplementary Figure 1C), giving rise to a smear because of the heterogeneous population of degraded fibers (Figure 5B, Lane 3). It was observed in the SDS-PAGE that there is an enrichment of the histones, suggesting the successful reconstitution of the 16xNCP (Figure 5C, Lane 5). However, the sample from the His-Trap purification was enriched in histones along with other bands, suggesting that the sample might have impurities and degraded products that were carried by during the whole protocol (Figure 5C, Lane 2). This could indicate that the degradation observed for the reconstituted 16x601 WIDOM (Figure 5A, Lane 3) and λ DNA (Figure 5B, Lane 3) could be due to these impurities. Conclusively, the standard protocol for the reconstitution of 16x601 WIDOM to form NCP arrays needed to be optimized in order to obtain full-length NCP arrays using λ phage DNA successfully.
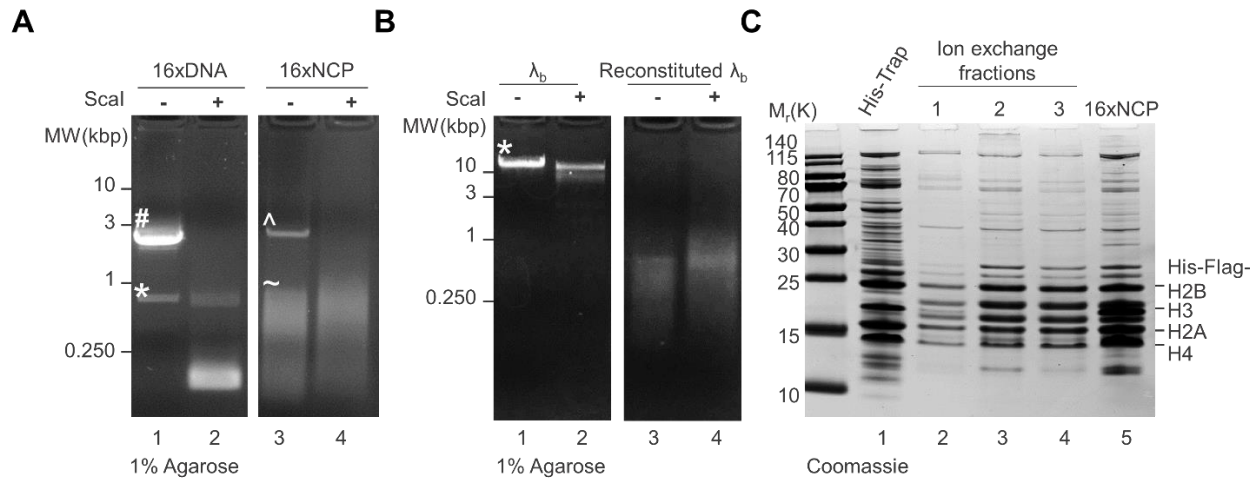
Figure 5: Reconstitution using pUC19 16x601 WIDOM and λ DNA. (A) Agarose gel represents the steps during reconstitution using pUC19 16x601 WIDOM. #, undigested 16x601 WIDOM at 2.8 kbp, *, carrier DNA at 1kb, ^, reconstituted 16x601 WIDOM, ~, degraded reconstituted 16x601 WIDOM **(B)** Agarose gel representing the steps during reconstitution using biotinylated λ phage DNA, *, undigested 48.5kbp biotinylated λ phage DNA that runs above 10kbp **(C)** Coomassie for the reconstitution using pUC19 16x601 WIDOM.

The first step in the optimization was to decrease the time of salt dialysis following the idea that the more prolonged incubation would be detrimental to the stability of the λ DNA fiber. Therefore, three time points for the salt dialysis were compared: 6 hours (not shown because it was too short for the reconstitution to be successful), 18 hours, and 24 hours (Figure 6A, 6B).

It was observed that the shorter time with successful reconstitution (18 hours of salt exchange) has less degradation of NCP arrays to some extent (Figure 6A, Lane 2) compared to the 24-hour sample. Moreover, in the 24-hour sample, the histones were not stoichiometric, and there was enrichment of other impurities (Figure 6B, Lane 2), suggesting yet again that the extra dialysis after salt exchange does not prove to be fruitful for the reconstitution. This supported the hypothesis that the His-Trap purification

contains impurities that lead to the degradation of DNA over time. Thus, decreasing the time that the DNA interacts with these impurities decreases the degradation.

Since DNA degradation was still present, we argued whether DNases were coming from the bacterial lysate among the impurities of the His-Trap (Oyama and Kubota, 1991). Therefore, an increasing concentration of EDTA was added during the salt dialysis to chelate divalent cations that might be used as cofactors by these enzymes . It was observed that there was not much of a difference in the samples with increasing concentrations of EDTA (Figure 6C, Lanes 2-4; Figure 6D, Lanes 2-4). To assess the stability of the fibers or we could gain more information on the degradation, we submitted these samples to TIRFM.

The λ DNA fibers used for this setup were biotinylated on both ends because it would give us an idea about the state of the degradation as full-length non-degraded fibers would be double tethered in the TIRFM (Figure 6E). It was observed that there were multiple double-tethered DNA fibers present, suggesting that there were still full-length fibers that were not degraded (Figure 6E, Lane1, Sytox Orange). However, some single tethered DNA fibers also suggested that partial degradation was still present (Figure 6E, Lane1, Sytox Orange & Figure 6F). Multiple fibers colocalized with the Qdot signal (Figure 6E, Lane 1, Overlay), suggesting nucleosome occupancy on these fibers (Figure 6G). Each Qdot signal represents one nucleosome (Figure 6E, Anti-Flag dot 705). The total length of the fibers was very heterogeneous, which could be due to the combination of partial degradation (for single tethered fibers) and the difference in the number of nucleosomes on the DNA (Figure 6E, Lane 1, Overlay). Taken altogether, this data suggests that, indeed, DNase degradation was detrimental for the chromatin reconstitution using λ DNA, whereas the 16x WIDOM sequence was not affected by it. Despite increasing EDTA helping in the case of λ DNA reconstitution, more improvements to the protocol had to be done to obtain a homogenous non-degraded chromatinized sample with more NCP occupancy.
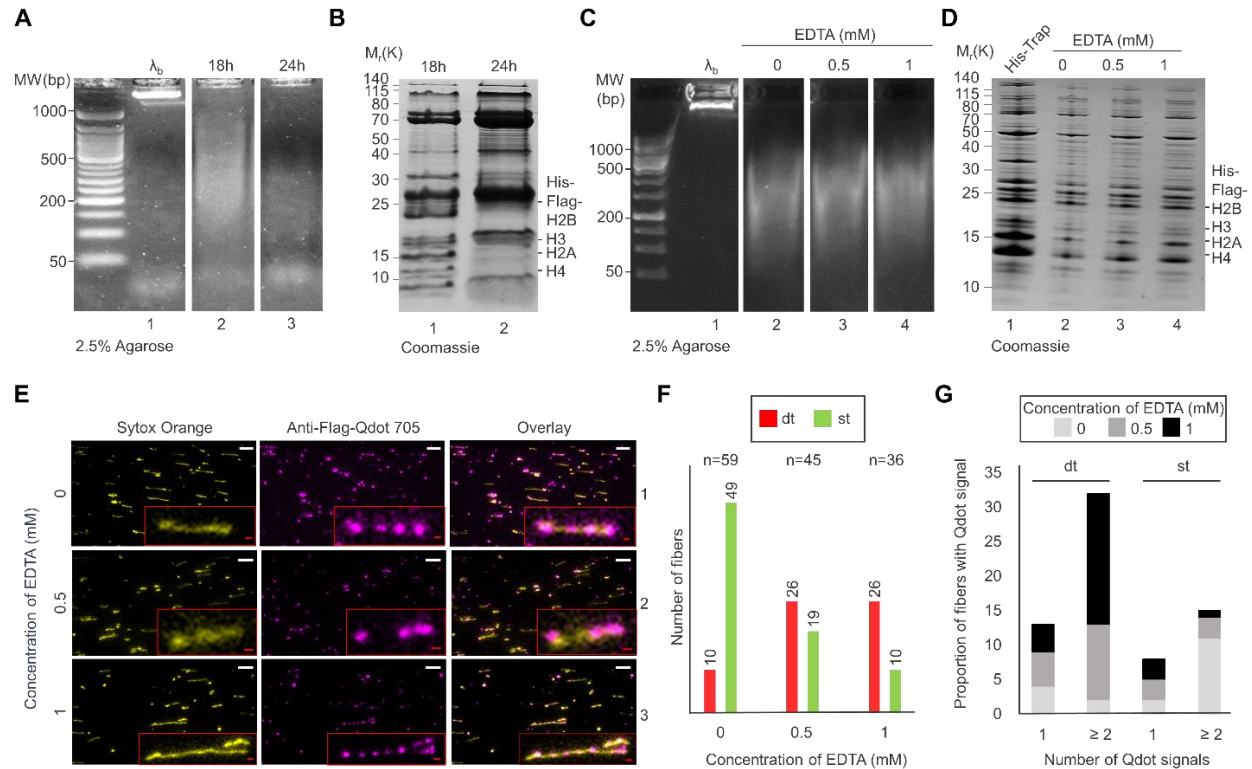
Figure 6: Optimization of reconstitution for the degradation of λ-DNA (A) Agarose gel for the reconstituted NCP array from biotinylated λ DNA after 18 and 24 hours. Lane 1, biotinylated λ DNA; Lanes 2, reconstituted NCP array from biotinylated λ DNA after 18 h; 3, reconstituted NCP array from biotinylated λ DNA after 18 hours after 24 h, respectively. **(B)** Coomassie for the reconstituted NCP array from biotinylated λ DNA. Lane 1, reconstituted NCP array after 18 hours; 2, reconstituted NCP array after 24 hours. Histones are not stoichiometric after 24 hours. **(C)** Agarose gel for the reconstituted NCP array from biotinylated λ DNA subjected to increasing concentration of EDTA during dialysis; Lane 1, biotinylated λ DNA; 2-4, different concentrations of EDTA. **(D)** Histone composition and stoichiometry for the samples with increasing concentration of EDTA. Lane 1, biotinylated λ DNA, 2-4 increasing EDTA concentration. **(E)** TIRFM for reconstituted NCP array from biotinylated λ DNA with increasing concentration of EDTA. Yellow, Sytox Orange labels λ DNA; Magenta, Anti-flag antibody labeled with Qdot 705. Scale bars: white, 6 μm. red: 1μm. **(F)** Quantification showing comparison for the number of double-tethered fibers (dt) vs. single-tethered fibers (st) with increasing concentration

of EDTA. n, total number of fibers **(G)** Quantification showing comparison for the number of double-tethered fibers (dt) and single-tethered fibers (st) with 1 or ≥2 Qdot signals.

4.2 Final protocol for reconstitution using λ DNA

To remove the impurities that degrade λ DNA completely, a whole modification of the standard protocol had to be done after His-Trap purification to purify the histones further. Attempts to apply ion-exchange chromatography with the λ chromatinized fibers were unsuccessful since the fibers were lost during this purification step (Supplementary Figure 1C). This could be because the ion exchange was performed in the AKTA system, and the long λ DNA fibers had to be subjected to high pressure due to the small size of the tubing in the system. Alternatively, the reconstituted fibers had to be exposed again to high salt during the ion exchange (eluting in more than 700 mM KCl), which could also be detrimental to their stability (Supplementary Figure 1C).

Therefore, an extra purification step was thus implemented after the His-Trap purification, including SEC, followed by concentration (Figure 7A, Supplementary Figure 2A). SEC segregates the histone octamers from the rest of the impurities and degraded products as it separates molecules based on size. The expected length of the octamer should be ~116 KDa, corresponding to the expected fraction between 80 mL- 85 mL (Figure 7B, Supplementary Figure 2B). However, the first attempt for SEC gave a prominent aggregate peak at 46-50 mL, followed by a long shoulder (fractions 55-68 mL) (Figure 7B). Moreover, no clear peak for the expected size of the HO was observed (Figure 7B). Since with this step, we wanted to eliminate the impurities from the His-Trap purification that led to λ DNA degradation, we decided to set up reconstitution with sequential fractions 46-50ml, 55-60 mL, 66-70 mL, 71-75 mL, and 80- 85 mL to find out which fraction gives the least amount of degradation but still the HO is intact, based on the stoichiometry of the histones (Figure 7B, Supplementary Figure 2B). It was observed that the DNA did not get degraded only for the reconstitutions, which were done using the fractions 66-70mL, 71-75mL, and 81-85mL from SEC (Figure 7C, Supplementary Figure 2C). The

histone sample was stoichiometric only for the input for reconstitution of the fractions 66-70 mL and 71-75 mL (Figure 7D, Supplementary Figure 2D). TIRFM analyses confirmed that the samples from the fractions 66-70 mL and 71-75 mL had less degradation since full-length (double-tethered) fibers were homogeneous and abundant (Figure 7E, Supplementary Figure 2F). Multiple fibers had ≥2 Qdot signals. A quantitative analysis (Figure 7E) depicted that more than 70% and 40% of the DNA fibers had ≥2 Qdot signals for reconstitution and Qdot signal, respectively, suggesting that the SEC did not affect the stability of the HO for a successful reconstitution into λ DNA. It was therefore decided to use the fractions 66-70 mL and 71-75 mL from SEC for the reconstitutions as they do not degrade DNA and the histone stoichiometry is closes to what is published as in (Visnapuu and Greene, 2009).
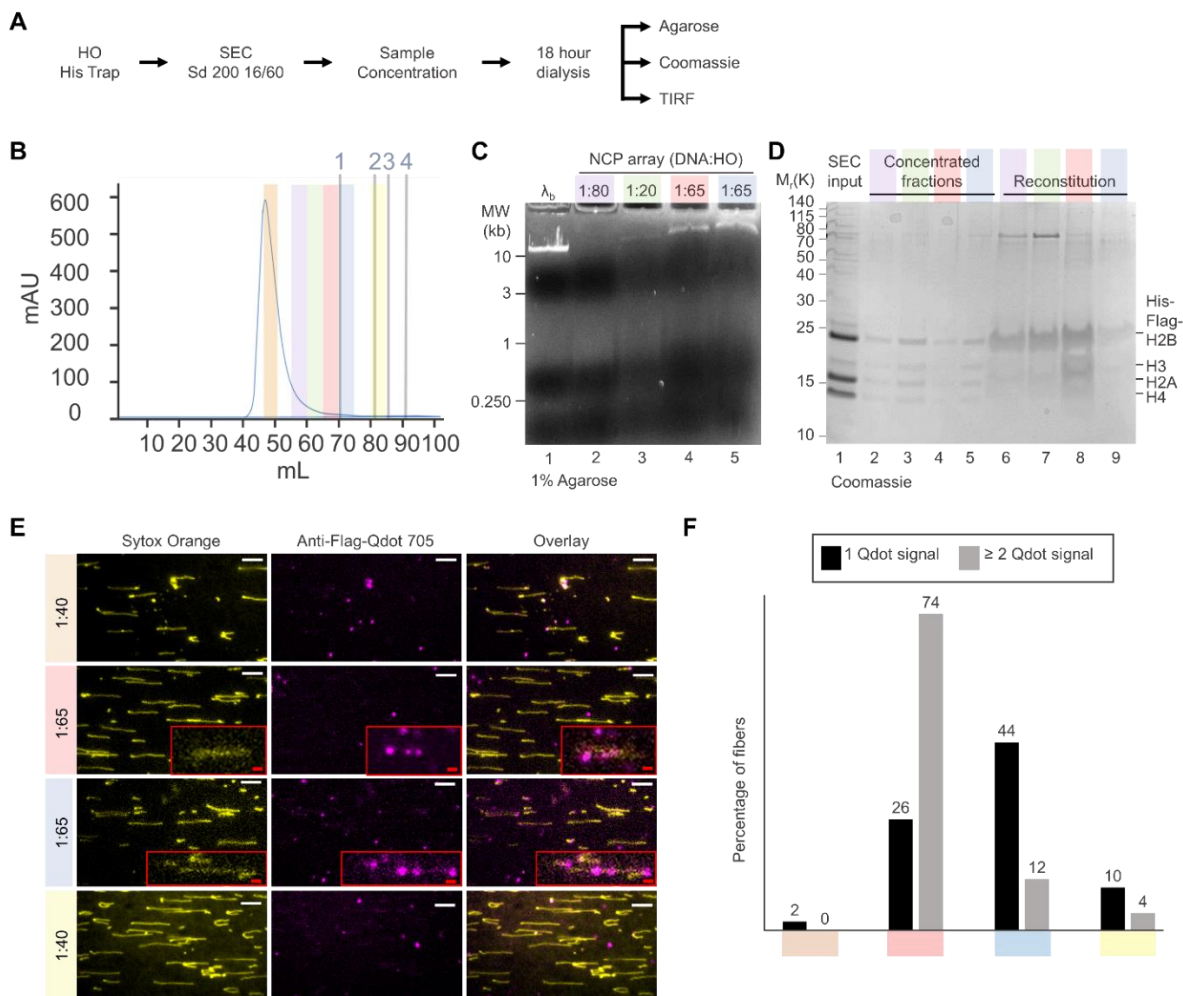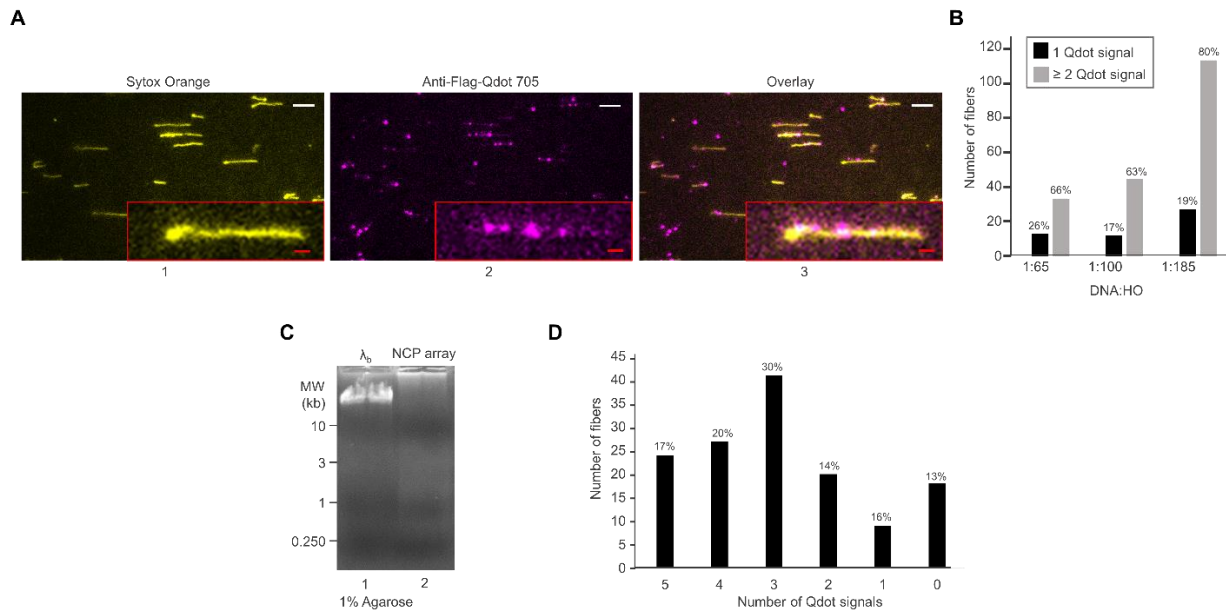
Figure 7: Optimization of the reconstitution by addition of SEC (A) Scheme for the optimized reconstitution for λ DNA. **(B)** SEC profile for the His-Trap purification. Markers are labeled with grey numbers. 1, Ferritin (440 kDa); 2, Aldolase (158 kDa); 3, Covoalbumin (75 kDa); 4, Ovalbumin (44 kDa). Fractions pooled together for the reconstitution are labeled with colours orange, 46-50mL; purple, 56-60mL; green, 61-65mL; red, 66-70mL; blue, 71-75mL; yellow, 81-85mL. **(C)** Agarose gel for the reconstitutions using different fractions from SEC (colors as in B). Lane1, biotinylated λ DNA. **(D)** Coomassie gel for the reconstitution using fractions from SEC (colors as in B) **(E)** TIRFM for reconstitutions using fractions from SEC (colors as in B). Different DNA:HO ratios were performed upon the availability of each fraction and are shown in the figure. Scale bars: white, 6 μm. red: 1μm. **(F)** Quantification for TIRFM in 8E comparing the percentage of fiber for each field with 1 or ≥2 Qdot signals. Numbers on the bar represent individual full-length chromatinized fibers (double-tethered).

Having achieved complete reconstitution for λ DNA without prominent degradation, single tethered DNA was used further in the experiments. The next step was to obtain a higher HO:DNA ratio, as it would be optimal to have five nucleosomes for each DNA fiber on average (as published by (Visnapuu and Greene, 2009)). Therefore, the fractions from 66 mL to 70 mL and 71 mL to 75 mL from SEC were concentrated and mixed to be used as a single input for the reconstitution (Figure 8A). A DNA:HO ratio of 1:185 could be obtained for this reconstitution with significantly higher NCP occupancy. It was observed that there were 60% of DNA fibers had ≥3 Qdot signals, as visualized in TIRFM (Figure 8A, 8B).

To increase nucleosome occupancy further in the chromatin fiber, we decided to increase the DNA:HO ratio to 1:300 (Visnapuu and Greene, 2009). This would involve the purification of a considerably higher amount of expressed protein (in total 20L). Therefore, we had to adjust the protocol in the first step for His-Trap purification to do it simultaneously in two AKTA systems (to maintain the same time in the purification and prevent histone octamer disassembly, Supplementary Figure 3B). The reconstitution was successful (Supplementary Figure 3A, 3B). However, the higher ratio proved detrimental

for the chromatinized template since aggregation was observed in TIRFM analysis and agarose (Supplementary Figure 3C).

Taken altogether, we conclude that the optimal DNA:HO ratio for chromatinized λ will be between 1:200 – 1:250 since a lower amount of histones would not give enough occupancy on the fibers on an average and higher than that would lead to aggregation of the fibers.

Figure 8: Optimization of ratio for reconstitution. (A) TIRFM for reconstitution using the fractions from 65 mL to 75 mL from SEC with DNA:HO ratio as 1:185. The total number of fibers was n= 139. Panel 1: DNA, Sytox Orange (yellow);s Panel 2, His-Flag H2B Qdot 705 (magenta); Panel 3, Overlay. **(B)** Quantitative analysis for the TIRFM showing the number of fibers that have 5, 4, 3, 2, 1, or 0 Qdot signal/s. Percentages for each type are shown on top of the bars. **(C)** Agarose gel for reconstitution using the fractions from 65 mL to 75 mL from SEC with DNA:HO as 1:185. Lane 1, biotinylated λ DNA; Lane2, Reconstitution, Scale bars: white, 6 μm. red: 1μm. **(D)** Quantitative analysis for the TIRFM showing number of fibers that have 5, 4, 3, 2, 1 or 0 number of Qdot signal/s for the sample with DNA:HO ratio of 1:185. Percentages for each type are shown on top of the bars.
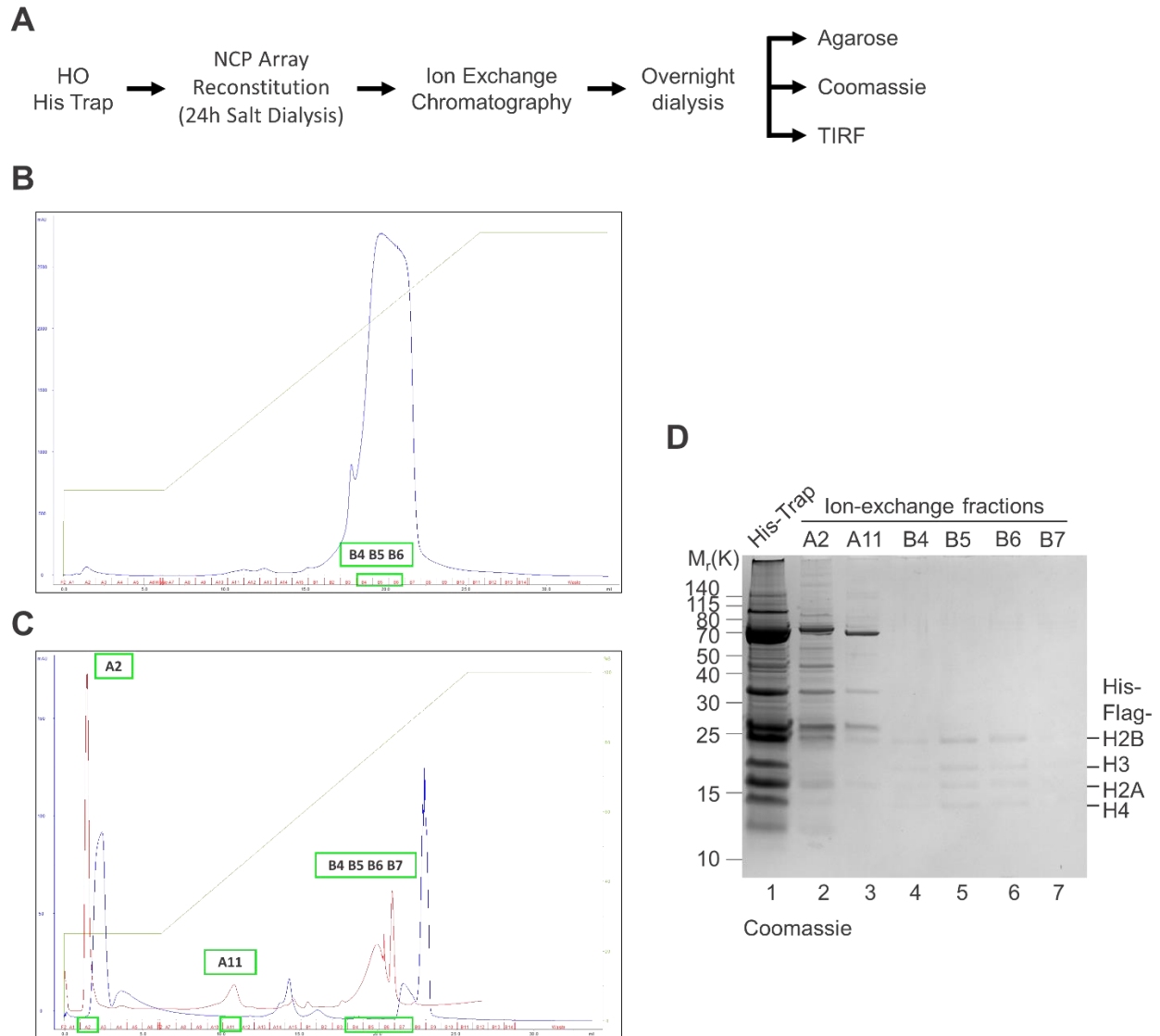
5. Concluding remarks and outlook

This project is the first step towards reconstituting the chromatin array for a template that would be useful for investigating the interaction of Lge1-Bre1 condensates with chromatin. The addition of an entirely different purification step to the existing protocol proved challenging given that the template that we were working with, λ DNA, already proves to be very sensitive to environmental and experimental procedures. Optimization involving the purification proved to be cumbersome as the histone octamers co-expressed are not as stable as when the histones are purified individually and then reconstituted, as described by (White, Suto and Luger, 2001). Even then, the reconstitution proved to be successful using the obtained method. The cloning of the histone tails also proved to be challenging as the sizes of the tails is very small. Nevertheless, cloning was successful for two constructs: the N-terminal tails of histones H2B and H3. Further cloning of the rest of the tails and purification needs to be done for investigating their interaction with the condensates.

Phase separation is a mechanism used by cellular environments to govern chromatin's organization and modification-related regulation. We still have far to go until the final experiments involving Lge-Bre1, to elucidate the molecular mechanism behind ubiquitination by the phase-separated condensates. How are Lge1-Bre1 condensates recruited to the chromatin fiber? How do the Lge1-Bre1 condensates act on chromatin? Do Lge1-Bre1 condensates regulate or alter chromatin compaction or dynamics? Do Lge1-Bre1 condensates move along chromatin fiber?

Addressing and understanding the molecular mechanisms behind membrane-bound compartments and their ability to be stable yet flexible to be fit to modulate such functions would give further insights into LLPS and extrapolate this knowledge to the macroscopic properties of phase separation and its regulation of chromatin.

6. Supplementary Figures

A

HO
His Trap → NCP Array
Reconstitution
(24h Salt Dialysis) → Ion Exchange
Chromatography → Overnight
dialysis →

→ Agarose
→ Coomassie
→ TIRF

B

C

D

Supplementary Figure 1: Standard protocol for chromatin reconstitution and applying it to λ DNA (A) Scheme for standard reconstitution implemented for 601 Widom reconstitution. **(B)** Ion-exchange chromatography for 16x601 WIDOM reconstitution using the protocol from Supplementary 1A. Blue: UV at 280nm for reconstituted biotinylated 16x601 WIDOM. Green: %concentration of buffer B. X-axis (red): fractions for the elution B4, B5, and B6 were the fractions taken for analysis. **(C)** Ion-exchange chromatography for λ DNA reconstitution using the protocol from Supplementary 1A. Blue: UV at 280nm biotinylated λ DNA, Red: reconstituted biotinylated λ DNA. Green: %concentration of

44

buffer B. X-axis (red): fractions for the elution A2, A11, B4, B5, B6, and B7 were the fractions taken for analysis. **(D)** Coomassie for the reconstituted samples for λ DNA after ion exchange. Lane 1, His-Trap purification.
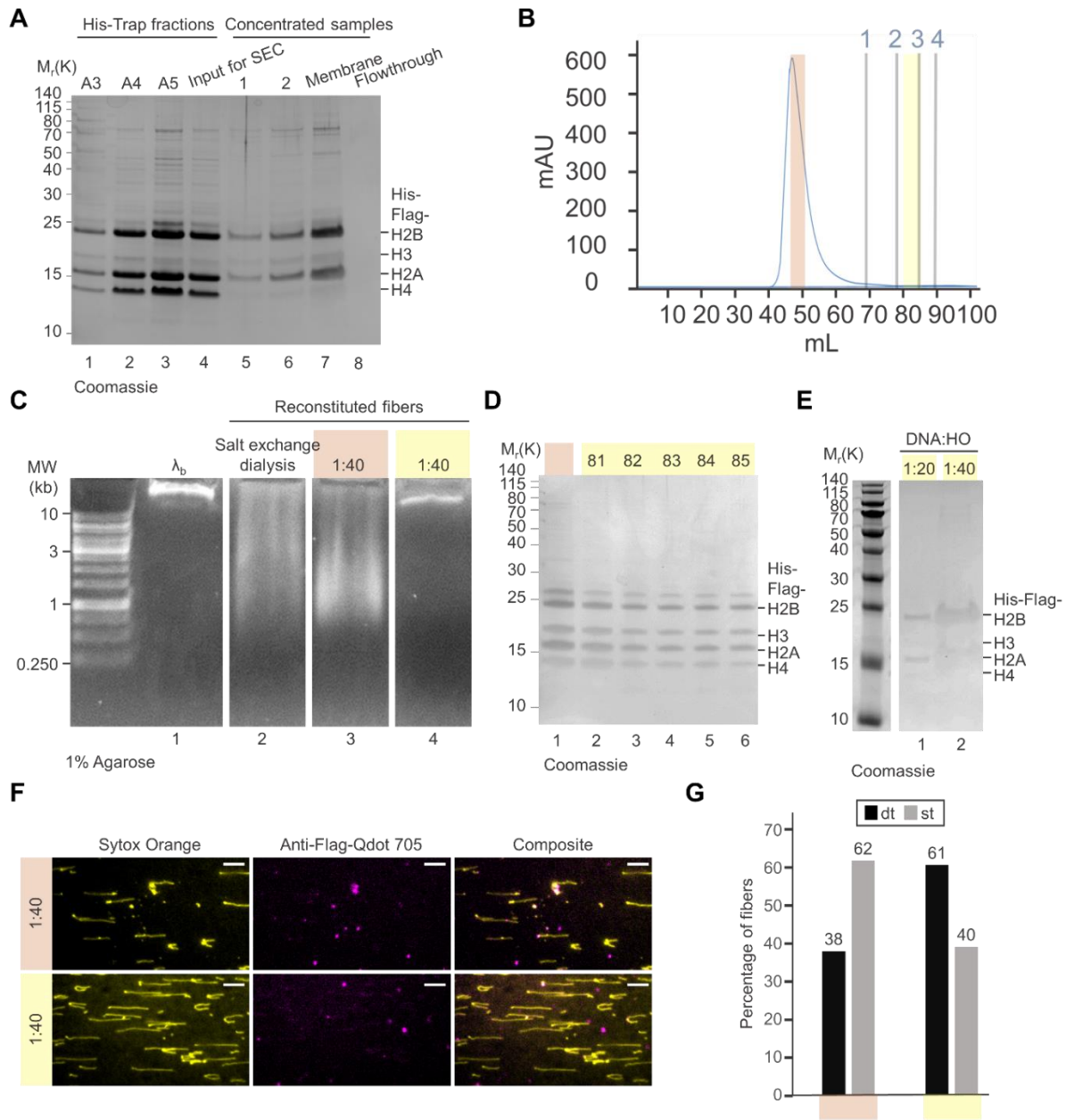
Supplementary Figure 2: Characterization of a new protocol for chromatin reconstitution. (A) Optimization for concentration after SEC. Lane 1, 2, 3: His-Trap fractions; 4, His-Trap purification; 5, sample concentrated to 500µL; 6, sample

concentrated to 250μL; 7, the sample taken by resuspending the protein bound to the membrane of the Amicon column; 8, the sample taken from the flowthrough after concentration. **(B)** SEC profile for the His-Trap purification. Markers are labeled with grey numbers, as in figure 6B. Fractions pooled together for the reconstitution are labeled with the colors orange, 46-50mL; blue: 81-85mL. **(C)** Agarose gel for the reconstitution comparing samples from standard protocol and fractions in Supplementary Figure 2B. Lane 1, biotinylated λ DNA, Lane 2: reconstituted sample using histones from His-Trap purification. **(D)** Coomassie for the fractions from Supplementary Figure 2B. Lane 2-6: 81-85mL. **(E)** Coomassie for reconstitution using fractions from Supplementary Figure 2B. **(F)** TIRFM for reconstitution using fractions from Supplementary Figure 2B. Scale bars: white, 6 μm. red: 1μm. **(G)** Quantification for the TIRFM in S2, F percentage of double-tethered (dt) vs. single-tethered (st) fibers in reconstitutions using fraction sets 1 and 2, respectively.
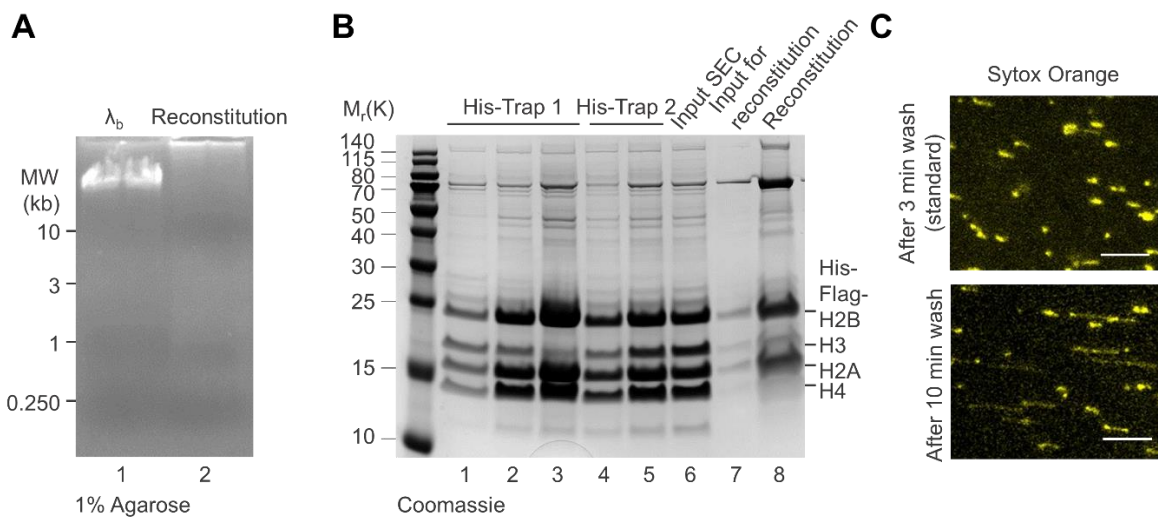
Supplementary Figure 3: Aggregation of fibers due to high concentration of HO (A) TIRFM for the reconstitution using histones from an expression volume of 20 L. Scale bars: white, 6 μm. red: 1μm. Only Sytox Orange channel is shown (labeling λ DNA). **(B)** Agarose from biotinylated λ DNA (Lane 1) and reconstitution using the histone sample from Supplementary Figure 3A. **(C)** Coomassie for the reconstitution using histone sample from Supplementary Figure 3A. Lane 1, 2, 3 and Lanes 4, 5, His=Trap purification sample from different systems. Lane 6= Input from His-Trap purification for SEC. Lane 7,

The fraction set 66-75 mL was taken for reconstitution after concentration; lane 8, Reconstituted NCP array after TCA precipitation. Scale bar: white, 5μm.

7. References

Ann Boija, A. et al. (2018) 'Transcription Factors Activate Genes through the Phase-Separation Capacity of Their Activation Domains In Brief Activation domains from a diverse array of mammalian and yeast transcription factors form phase-separated condensates with Mediator to activate gene expression', Cell, 175, pp. 1842-1855.e16. Available at: https://doi.org/10.1016/j.cell.2018.10.042.

Baldi, S., Korber, P. and Becker, P.B. (2020) 'Beads on a string—nucleosome array arrangements and folding of the chromatin fiber', Nature Structural & Molecular Biology 2020 27:2, 27(2), pp. 109–118. Available at: https://doi.org/10.1038/s41594-019-0368-x.

Banani, S.F. et al. (2017a) 'Biomolecular condensates: Organizers of cellular biochemistry', Nature reviews. Molecular cell biology, 18(5), p. 285. Available at: https://doi.org/10.1038/NRM.2017.7.

Bannister, A.J. and Kouzarides, T. (2011) 'Regulation of chromatin by histone modifications', Cell Research, 21(3), p. 381. Available at: https://doi.org/10.1038/CR.2011.22.

Boehning, M. et al. (2018) 'RNA polymerase II clustering through carboxy-terminal domain phase separation', Nature Structural & Molecular Biology 2018 25:9, 25(9), pp. 833–840. Available at: https://doi.org/10.1038/s41594-018-0112-y.

Bussiek, M. et al. (2007) 'Organisation of nucleosomal arrays reconstituted with repetitive African green monkey α-satellite DNA as analysed by atomic force microscopy', undefined, 37(1), pp. 81–93. Available at: https://doi.org/10.1007/S00249-007-0166-Y.

Callis, J. (2014) 'The ubiquitination machinery of the ubiquitin system', The arabidopsis book, 12, p. e0174. Available at: https://doi.org/10.1199/TAB.0174.

Candiano, G. et al. (2004) 'Blue silver: A very sensitive colloidal Coomassie G-250 staining for proteome analysis', ELECTROPHORESIS, 25(9), pp. 1327–1333. Available at: https://doi.org/10.1002/ELPS.200305844.

Cao, J. and Yan, Q. (2012) 'Histone ubiquitination and deubiquitination in transcription, DNA damage response, and cancer', Frontiers in Oncology, 2(MAR), p. 26. Available at: https://doi.org/10.3389/FONC.2012.00026/XML/NLM.

Chavez, M.S. et al. (2012) 'The conformational flexibility of the C-terminus of histone H4 promotes histone octamer and nucleosome stability and yeast viability', Epigenetics and

Chromatin, 5(1), pp. 1–20. Available at: https://doi.org/10.1186/1756-8935-5-5/FIGURES/9.

Ciechanover, A. and Schwartz, A.L. (1998) 'The ubiquitin-proteasome pathway: The complexity and myriad functions of proteins death', Proceedings of the National Academy of Sciences of the United States of America, 95(6), p. 2727. Available at: https://doi.org/10.1073/PNAS.95.6.2727.

Collins, B.E. et al. (2014) 'DNA curtains: novel tools for imaging protein-nucleic acid interactions at the single-molecule level', Methods in cell biology, 123, pp. 217–234. Available at: https://doi.org/10.1016/B978-0-12-420138-5.00012-4.

Cucinotta, C.E. et al. (2015) 'The Nucleosome Acidic Patch Regulates the H2B K123 Monoubiquitylation Cascade and Transcription Elongation in Saccharomyces cerevisiae', PLOS Genetics, 11(8), p. e1005420. Available at: https://doi.org/10.1371/JOURNAL.PGEN.1005420.

Davidson, I.F. et al. (2016) 'Rapid movement and transcriptional re-localization of human cohesin on DNA', The EMBO Journal, 35(24), pp. 2671–2685. Available at: https://doi.org/10.15252/EMBJ.201695402.

Deng, Z.H. et al. (2020) 'The Bre1/Rad6 machinery: writing the central histone ubiquitin mark on H2B and beyond', Chromosome Research 2020 28:3, 28(3), pp. 247–258. Available at: https://doi.org/10.1007/S10577-020-09640-3.

Elmore, Z.C. et al. (2014) 'Histone H2B ubiquitination promotes the function of the anaphase-promoting complex/cyclosome in Schizosaccharomyces pombe', G3: Genes, Genomes, Genetics, 4(8), pp. 1529–1538. Available at: https://doi.org/10.1534/G3.114.012625/-/DC1.

Fazio, T. et al. (2008) 'DNA Curtains and Nanoscale Curtain Rods: High-Throughput Tools for Single Molecule Imaging', Langmuir : the ACS journal of surfaces and colloids, 24(18), p. 10524. Available at: https://doi.org/10.1021/LA801762H.

Finkelstein, I.J., Visnapuu, M.L. and Greene, E.C. (2010) 'Single-molecule imaging reveals mechanisms of protein disruption by a DNA translocase', Nature 2010 468:7326, 468(7326), pp. 983–987. Available at: https://doi.org/10.1038/nature09561.

Fish, K.N. (2009) 'Total Internal Reflection Fluorescence (TIRF) Microscopy', Current Protocols in Cytometry, 50(1), pp. 12.18.1-12.18.13. Available at: https://doi.org/10.1002/0471142956.CY1218S50.

Galganski, L., Urbanek, M.O. and Krzyzosiak, W.J. (2017) 'Nuclear speckles: molecular organization, biological function and role in disease', Nucleic Acids Research, 45(18), p. 10350. Available at: https://doi.org/10.1093/NAR/GKX759.

Gallego, L.D. et al. (2020) 'Phase separation directs ubiquitination of gene-body nucleosomes', Nature 2020 579:7800, 579(7800), pp. 592–597. Available at: https://doi.org/10.1038/s41586-020-2097-z.

Ghoneim, M., Fuchs, H.A. and Musselman, C.A. (2021) 'Histone Tail Conformations: A Fuzzy Affair with DNA', Trends in Biochemical Sciences, 46(7), pp. 564–578. Available at: https://doi.org/10.1016/J.TIBS.2020.12.012.

Gibson, B.A. et al. (2019) 'Organization of Chromatin by Intrinsic and Regulated Phase Separation', Cell, 179(2), pp. 470-484.e21. Available at: https://doi.org/10.1016/j.cell.2019.08.037.

Hwang, W.W. et al. (2003) 'A conserved RING finger protein required for histone H2B monoubiquitination and cell size control', Molecular cell, 11(1), pp. 261–266. Available at: https://doi.org/10.1016/S1097-2765(02)00826-2.

Hyman, A.A., Weber, C.A. and Jülicher, F. (2014) 'Liquid-liquid phase separation in biology', Annual review of cell and developmental biology, 30, pp. 39–58. Available at: https://doi.org/10.1146/ANNUREV-CELLBIO-100913-013325.

Koken, M.H.M. et al. (1991) 'Structural and functional conservation of two human homologs of the yeast DNA repair gene RAD6.', Proceedings of the National Academy of Sciences of the United States of America, 88(20), p. 8865. Available at: https://doi.org/10.1073/PNAS.88.20.8865.

Kornberg, R.D. (1974) 'Chromatin structure: A repeating unit of histones and DNA', Science, 184(4139), pp. 868–871. Available at: https://doi.org/10.1126/SCIENCE.184.4139.868/ASSET/F767CB17-9373-448B-A058-D0598FEFAF69/ASSETS/SCIENCE.184.4139.868.FP.PNG.

Laemmli, U.K. (1970) 'Cleavage of structural proteins during the assembly of the head of bacteriophage T4', Nature, 227(5259), pp. 680–685. Available at: https://doi.org/10.1038/227680A0.

Li, C. et al. (2011) 'FastCloning: A highly simplified, purification-free, sequence- and ligation-independent PCR cloning method', BMC Biotechnology, 11(1), pp. 1–10. Available at: https://doi.org/10.1186/1472-6750-11-92/FIGURES/6.

Li, C. et al. (2019) 'Study on host-seeking behavior and chemotaxis of entomopathogenic nematodes using Pluronic F-127 gel', Journal of Invertebrate Pathology, 161, pp. 54–60. Available at: https://doi.org/10.1016/J.JIP.2019.01.004.

Lowary, P.T. and Widom, J. (1998) 'New DNA sequence rules for high affinity binding to histone octamer and sequence-directed nucleosome positioning', Journal of molecular biology, 276(1), pp. 19–42. Available at: https://doi.org/10.1006/JMBI.1997.1494.

Lusser, A. and Kadonaga, J.T. (2004) 'Strategies for the reconstitution of chromatin', Nature Methods 2004 1:1, 1(1), pp. 19–26. Available at: https://doi.org/10.1038/nmeth709.

Lyon, A.S., Peeples, W.B. and Rosen, M.K. (2021) 'A framework for understanding functions of biomolecular condensates on molecular to cellular scales', Nature reviews. Molecular cell biology, 22(3), p. 215. Available at: https://doi.org/10.1038/S41580-020-00303-Z.

Mariño-Ramírez, L. et al. (2007) 'Histone structure and nucleosome stability NIH Public Access'.

Mattheyses, A.L., Simon, S.M. and Rappoport, J.Z. (2010) 'Imaging with total internal reflection fluorescence microscopy for the cell biologist', Journal of cell science, 123(Pt 21), pp. 3621–3628. Available at: https://doi.org/10.1242/JCS.056218.

McGinty, R.K. and Tan, S. (2015) 'Nucleosome structure and function', Chemical Reviews, 115(6), pp. 2255–2273. Available at: https://doi.org/10.1021/CR500373H/ASSET/IMAGES/LARGE/CR-2014 00373H_0014.JPEG.

Morin, J.A. et al. (2020) 'Surface condensation of a pioneer transcription factor on DNA', bioRxiv, p. 2020.09.24.311712. Available at: https://doi.org/10.1101/2020.09.24.311712.

Nakanishi, S. et al. (2009) 'Histone H2BK123 monoubiquitination is the critical determinant for H3K4 and H3K79 trimethylation by COMPASS and Dot1', The Journal of Cell Biology, 186(3), p. 371. Available at: https://doi.org/10.1083/JCB.200906005.

Nurse, N.P. et al. (2013) 'Clipping of Flexible Tails of Histones H3 and H4 Affects the Structure and Dynamics of the Nucleosome', Biophysical Journal, 104(5), pp. 1081–1088. Available at: https://doi.org/10.1016/J.BPJ.2013.01.019.

Oyama, M. and Kubota, K. (1991) 'Inhibition by EDTA and enhancement by divalent cations or polyamines of the dithiothreitol-induced activation of adenylate cyclase in the

cellular slime mold, Dictyostelium discoideum', Biochimica et biophysica acta, 1092(1), pp. 85–88. Available at: https://doi.org/10.1016/0167-4889(91)90180-6.

Quina, A.S., Buschbeck, M. and di Croce, L. (2006) 'Chromatin structure and epigenetics', Biochemical Pharmacology, 72(11), pp. 1563–1569. Available at: https://doi.org/10.1016/J.BCP.2006.06.016.

Reynolds, P. et al. (1990) 'The rhp6+ gene of Schizosaccharomyces pombe: a structural and functional homolog of the RAD6 gene from the distantly related yeast Saccharomyces cerevisiae.', The EMBO Journal, 9(5), pp. 1423–1430. Available at: https://doi.org/10.1002/J.1460-2075.1990.TB08258.X.

Rosa, S. and Shaw, P. (2013) 'Insights into Chromatin Structure and Dynamics in Plants', Biology 2013, Vol. 2, Pages 1378-1410, 2(4), pp. 1378–1410. Available at: https://doi.org/10.3390/BIOLOGY2041378.

Sambrook, J., Fritsch, E.F. and Maniatis, T. (1989) 'Molecular cloning: a laboratory manual.', Molecular cloning: a laboratory manual. [Preprint], (Ed. 2).

Sanulli, S. et al. (2019) 'HP1 reshapes nucleosome core to promote phase separation of heterochromatin', Nature, 575(7782), pp. 390–394. Available at: https://doi.org/10.1038/S41586-019-1669-2.

Shakya, A. et al. (2020a) 'Liquid-Liquid Phase Separation of Histone Proteins in Cells: Role in Chromatin Organization', Biophysical Journal, 118(3), pp. 753–764. Available at: https://doi.org/10.1016/J.BPJ.2019.12.022.

Shakya, A. et al. (2020b) 'Liquid-Liquid Phase Separation of Histone Proteins in Cells: Role in Chromatin Organization', Biophysical Journal, 118(3), pp. 753–764. Available at: http://www.cell.com/article/S0006349519344078/fulltext (Accessed: 29 September 2022).

Song, Y.H. and Ahn, S.H. (2010) 'A Bre1-associated protein, large 1 (Lge1), promotes H2B ubiquitylation during the early stages of transcription elongation', The Journal of biological chemistry, 285(4), pp. 2361–2367. Available at: https://doi.org/10.1074/JBC.M109.039255.

Turco, E. et al. (2015) 'Monoubiquitination of histone H2B is intrinsic to the Bre1 RING domain-Rad6 interaction and augmented by a second Rad6-binding site on Bre1', The Journal of biological chemistry, 290(9), pp. 5298–5310. Available at: https://doi.org/10.1074/JBC.M114.626788.

Ura, K. and Kaneda, Y. (2001) 'Reconstitution of chromatin in vitro', Methods in molecular biology (Clifton, N.J.), 181, pp. 309–325. Available at: https://doi.org/10.1385/1-59259-211-2:309.

Visnapuu, M.L. and Greene, E.C. (2009) 'Single-molecule imaging of DNA curtains reveals intrinsic energy landscapes for nucleosome deposition', Nature structural & molecular biology, 16(10), pp. 1056–1062. Available at: https://doi.org/10.1038/NSMB.1655.

Wagh, K., Garcia, D.A. and Upadhyaya, A. (2021) 'Phase separation in transcription factor dynamics and chromatin organization', Current Opinion in Structural Biology, 71, pp. 148–155. Available at: https://doi.org/10.1016/J.SBI.2021.06.009.

Wang, C.Y. et al. (2011) 'The C-Terminus of Histone H2B Is Involved in Chromatin Compaction Specifically at Telomeres, Independently of Its Monoubiquitylation at Lysine 123', PLOS ONE, 6(7), p. e22209. Available at: https://doi.org/10.1371/JOURNAL.PONE.0022209.

White, C.L., Suto, R.K. and Luger, K. (2001) 'Structure of the yeast nucleosome core particle reveals fundamental changes in internucleosome interactions', The EMBO Journal, 20(18), p. 5207. Available at: https://doi.org/10.1093/EMBOJ/20.18.5207.

Wilchek, M. and Bayer, E.A. (1990) 'Introduction to avidin-biotin technology', Methods in enzymology, 184(C), pp. 5–13. Available at: https://doi.org/10.1016/0076-6879(90)84256-G.

Wood, A. et al. (2003) 'Bre1, an E3 Ubiquitin Ligase Required for Recruitment and Substrate Selection of Rad6 at a Promoter', Molecular Cell, 11(1), pp. 267–274. Available at: https://doi.org/10.1016/S1097-2765(02)00802-X.

Yardimci, H. et al. (2012) 'Single-molecule analysis of DNA replication in Xenopus egg extracts', Methods (San Diego, Calif.), 57(2), p. 179. Available at: https://doi.org/10.1016/J.YMETH.2012.03.033.

Zhang, F. and Yu, X. (2011) 'WAC, a functional partner of RNF20/40, regulates histone H2B ubiquitination and gene transcription', Molecular cell, 41(4), p. 384. Available at: https://doi.org/10.1016/J.MOLCEL.2011.01.024.

Zhu, B., Zheng, Y., Pham, A.D., et al. (2005) 'Monoubiquitination of human histone H2B: The factors involved and their roles in HOX gene regulation', Molecular Cell, 20(4), pp. 601–611. Available at: https://doi.org/10.1016/J.MOLCEL.2005.09.025.